Spectroscopic CW-EPR and HYSCORE investigations of Cu2+ and O2− species in copper doped nanoporous calcium aluminate (12CaO·7Al2O3)

UNIVERSITÀ DEGLI STUDI DI TORINO

Spectroscopic CW-EPR and HYSCORE Investigations of Cu^{2+} and O_2^- Species in Copper Doped Nanoporous Calcium Aluminate ($12CaO \cdot 7Al_2O_3$)

Sara Maurelli,[a] Monika Ruszak,[b] Stefan Witkowski,[b] Piotr Pietrzyk,[b] Mario Chiesa,*[a] Zbigniew Sojka*[b]

Continuous wave (CW) and pulse electron paramagnetic resonance in variant of hyperfine sublevel correlation spectroscopy (HYSCORE) were used for obtaining structural information concerning speciation and local environment of alien Cu^{2+} and native O_2^- ions encaged in copper doped nanoporous $12CaO{\cdot}7Al_2O_3$ (mayenite). The samples were prepared by solid-state reaction and characterized by means of XRD, SEM, and Raman techniques. X-band CW-EPR spectra showed that three different Cu^{2+} species together with paramagnetic extraframework O_2^- anions were present in the mayenite sample, whereas extraframework OH^- anions were revealed by Raman spectroscopy. ^{27}Al HYSCORE provided evidence for the interaction of Cu^{2+} ions with the mayenite framework. Superhyperfine interaction of the Cu^{2+} ions with proximal (d_{Cu-OH} = 2.4 Å) and distal (d_{Cu-OH} = 5.0 Å) OH^- anions, located in the same and the nearby cage, respectively, was resolved by means of ^1H HYSCORE spectra. A different situation holds for the encaged O_2^- radicals, which were found to be sitting on the Ca^{2+} ions and exhibited only a weak superhyperfine interaction of 1 MHz with the $^{27}Al^{3+}$ framework ions.

Introduction

Nano-sized and nano-porous oxides exhibiting specific physical and chemical properties, which are distinctly different from those related to bulk solids, are nowadays attracting wide research interest.[1,2,3] Their unique size-dependent features open new possibilities for producing advanced materials, molecular sieves and exclusive catalysts that can be tailored to specific applications.[4,5]

Mayenite ($12CaO{\cdot}7Al_2O_3$) is an unique nano-porous oxide, characterized by the positively charged calcium aluminate framework that is counterbalanced by extra-lattice O^{2-} ions. Such free oxide ions are responsible for the ionic conduction,[6] and can further be partially or completely replaced by various guest anions such as O_2^-, O_2^{2-}, O^-, OH^-, H^- or even electrons.[7] In the latter case the resultant electride material $[Ca_{24}Al_{28}O_{64}]^{4+}(4e^-)$ exhibits unique combination of optical transparency and high electronic conductivity.7,[8] Another spectacular feature of mayenite is connected with its remarkable capacity of storing and stabilization of O_2^- radical ions within the cages in a wide concentration range.[9] They have recently been characterized by EPR spectroscopy using ^{17}O-enriched oxygen[10] and proposed to be involved in catalytic processes.[11]

Mayenite, pristine or promoted by appropriate doping, is an attractive total oxidation catalyst for volatile organic compounds,[12] for selective high-temperature N_2O removal from process gases in nitric acid plants,[11] and for diesel soot combustion.[13] In the latter case its activity can be improved substantially by doping with transition-metal ions. Among several investigated cations, such as Fe, Ni, Co, Cr or Cu, copper has led to the highest increase of the catalyst activity. This observation has been associated with reactivity enhancement of the occluded O_2^- species, conferred by the copper dopant[13]. The extra-lattice oxygen species were also proposed to be involved in an intrafacial recombination process of the peroxide intermediates produced in high temperature N_2O decomposition[11].

In this paper we use a combination of CW and pulse EPR techniques to describe the local environment of the native superoxide radicals and speciation of alien copper(II) ions accommodated in the mayenite matrix.

Experimental details

Synthesis

Polycrystalline $12CaO{\cdot}7Al_2O_3$ samples were obtained by conventional high temperature solid-state reaction between analytical grade $CaCO_3$ (Aldrich) and γ-Al_2O_3 (Aldrich). Both reagents were carefully mixed in the stoichiometric ratio ($CaO:Al_2O_3$ = 12:7) by grinding in an electromechanical agate mortar for about 6 h. Homogenized powder was sintered at 1623 K in platinum crucibles for 6 h in air. Copper containing samples were obtained by impregnation of the synthesized mayenite with an ethanol solution of copper(II) nitrate, followed by calcination at 1173 K for 0.5 h. The Cu/Ca ratio in the resultant samples corresponded approximately to one copper cation per unit cell of the mayenite.

Characterization of the samples

The phase purity of the samples was confirmed by means of X-ray diffraction using a Philips XPERT PRO PW1710 diffractometer with CuKα radiation in the Bragg-Brentano

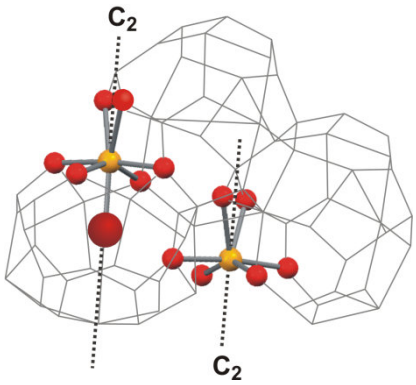

Fig. 1 Fragment of the $12CaO{\cdot}7Al_2O_3$ structure showing two neighboring nanocages with two types of local environment for the divalent Ca(Cu) cations.

geometry. Powder samples were scanned in the range of 2θ between 10° and 80° with the resolution of 0.02°. The morphology of the samples was examined with a Hitachi S-4700 scanning electron microscope equipped with a Noran Vantage microanalysis system.

Raman spectra were recorded with the spectral resolution of 4 cm^{-1} by means of a InVia Renishaw spectrometer integrated with confocal microscope, equipped with a CCD detector and a 360 mW laser operating at the wavelength of 785 nm.

CW-EPR spectra were recorded at liquid nitrogen and room temperatures on a Bruker ELEXSYS 500 spectrometer working at X-band with 100 kHz modulation. The microwave power of 1 – 200 mW and the modulation amplitude of 0.2 – 0.4 mT were applied. The spectra processing was performed with the software provided by Bruker, while for computer simulation of the powder spectra the EPRsim32 program was used.[14]

Pulse EPR experiments were performed on an ELEXSYS 580 Bruker spectrometer (at the microwave frequency of 9.76 GHz) equipped with a liquid-helium cryostat from Oxford Inc. All experiments were performed at 10 K. The magnetic field was measured by means of a Bruker ER035M NMR gaussmeter.

Electron spin echo (ESE) detected EPR experiments were carried out with the pulse sequence: $\pi/2-\tau-\pi-\tau$–echo, with microwave pulse lengths $t_{\pi/2}$ = 16 ns and t_π = 32 ns and a τ value of 200 ns. Hyperfine sublevel correlation (HYSCORE) experiments[15] were carried out with the pulse sequence $\pi/2-\tau-\pi/2-t_1-\pi-t_2-\pi/2-\tau$–echo with the microwave pulse length $t_{\pi/2}$ = 16 ns and t_π = 16 ns. The time intervals t_1 and t_2 were varied in steps of 16 ns starting from 96 ns to 3296 ns. In order to avoid blind spot effects different τ values were chosen, which are specified in the figure captions. An eight-step phase cycle was used for eliminating unwanted echoes.

The time traces of the HYSCORE spectra were baseline corrected with a third-order polynomial, apodized with a Hamming window and zero filled. After two-dimensional Fourier transformation, the absolute value spectra were calculated. The spectra were added for the different τ values in order to eliminate blind-spot effects. The HYSCORE spectra were simulated using a program developed at the ETH Zurich.[16]

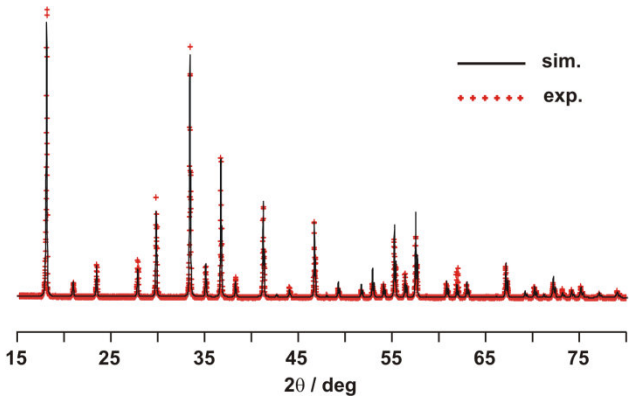

Fig. 2 The X-ray diffraction pattern of Cu-doped mayenite sample (experimental data - doted line, Rietveld profile - solid line).

Results and discussion

Mayenite forms cubic crystals exhibiting the *I*-43*d* space group symmetry and a large lattice constant of about 12 Å.[17] The

stoichiometric chemical formula for the unit cell can formally be expressed as $[Ca_{24}Al_{28}O_{64}]^{4+}(2O^{2-})$. The positively charged framework is arranged in 12 cages similar to those of the sodalite unites with an average charge of +1/3*e* each, which is compensated by two extra-lattice oxygen anions ($12\times1/3e + 2\times(-2)e = 0$), distributed over different cages. Each single cage consists of 16 oxygen ions, 8 tetracoordinated aluminum ions and 6 hexacoordinated calcium ions. The rather irregular Ca polyhedron has four shorter bonds (2.35 and 2.39 Å) in an approximately planar configuration and two longer bonds (2.59 Å) which are connected to the Al tetrahedron.[17] A possible seven-fold coordination of Ca^{2+} (Fig. 1) may arise from the presence of an extraframework anion in the close vicinity of the calcium ions (2.73 Å). The interaction between both moieties, as it can be judged from the corresponding interatomic distance, is sufficient to be categorized as a proper chemical bond, and obviously cannot be disregarded in the context of its impact on the magnetic parameters (vide infra). As a result such peculiar structure of the mayenite allows for distinction of two generic types of the coordination polyhedra of calcium ions (a six-fold and seven-fold one, shown in Fig. 1). In both cases the site symmetry of the Ca^{2+} ions can be approximated as C_{2v} with the two-fold axis placed along a S_4 axis connecting two Ca atoms.

Whereas the framework of mayenite is chemically rigid, the composition of the extraframwork species can be relatively easily modified by appropriate chemical treatment.[10,18] The inner size of the mayenite cages is approximately equal to 4 Å, and they are connected to 8 other cages by 3.5 Å openings, restraining direct access of guest molecules, essentially to mono-atomic species. However, diatomic charge-balancing anions such as OH^-, O_2^- or O_2^{2-} can also be formed *in situ* (i.e. within the cages), as discussed elsewhere in more detail.8·[18] Speciation of the extraframework anions together with the remarkable anisotropy of the atomic displacement parameters (ADP ellipsoids) point to considerable disorder of the calcium nearest environment, giving rise to broading of the spectral lines (vide infra).

Powder diffraction

The XRD pattern of the samples (Fig. 2) indicated that the synthesized material consists primarily of the mayenite structure. Yet, a more detailed Rietveld analysis showed that beside the dominant mayenite phase (6287 ICSD), a small admixture of $Ca_3Al_2O_6$ (1.3 ± 0.6%) phase (1841 ICSD) was also detected. The mean weighted dimension of the crystallinity zone of the mayenite phase obtained from the Rietveld calculations was equal to 0.3 μm. The lattice constant of the Cu-bearing samples, equal to a = 11.974 Å, was found to be distinctly smaller than that of undoped (copper-free) mayenite (a = 11.998 Å). Such cell contraction can be assigned to substitution of a smaller Cu^{2+} (0.73 Å) cation for a larger Ca^{2+} (1.0 Å radius) one, implying a successful incorporation of copper ions into the mayenite framework in the form of $Cu_{Ca}^{\times}$ centers (vide infra).

Scanning electron microscopy

The SEM morphology of the samples shown in Fig. 3 revealed the presence of a well sintered coarse solid composed of round crystallites, which are interconnected by broad necks. The average particle size obtained from analysis of the SEM pictures was in the range of 0.3 to 1 μm. Corroborative EDX analysis showed that the molar ratio Ca:Al, equal to 12.0:14.8, is very close to the mayenite stoichiometry, in agreement with XRD data.

Raman spectroscopy

The presence of the extraframework O_2^-, OH^-, and O_2^{2-} anions encaged within the mayenite matrix was revealed by Raman spectroscopy. The spectra are presented in Fig. S1 (Supplementary Information), whereas positions of the main Raman bands are summarized in Table 1. The low frequency spectral region below 400 cm^{-1} along with the bands at 519, 772, and 913 cm^{-1} were assigned to framework vibration modes.[15,19,20] The band due to the clathrated peroxide ions (O_2^{2-}) was situated at 771 cm^{-1},[21] whereas the band at 1127 cm^{-1} was assigned to superoxide radicals (O_2^-).[10] In the region of the hydroxyl groups (3500 – 3600 cm^{-1}), there was a strong band at 3573 cm^{-1}, which corresponds to extraframework OH^- anions.[22]

CW-EPR results

Powder CW-EPR spectrum of the copper-free mayenite shows an orthorhombic EPR spectrum (Fig. 4, solid line)

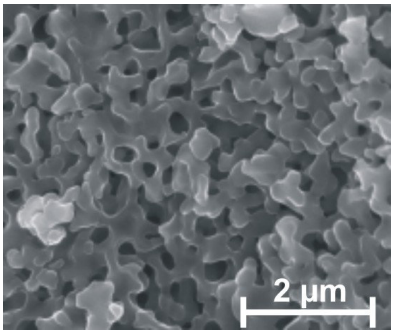

Fig. 3 Typical morphology of the mayenite sample as revealed by scanning electron microscopy imaging with secondary electrons.

Table 1 Principal bands observed in the Raman spectra of the Cu-bearing mayenite sample

Raman shift / cm^{-1}	Assignement	Assignement references
519	Ca–O–Al lattice vibration	19
772	A_1, Al–O lattice vibration	20
913	T_2, Al–O lattice vibration	20
771	extraframework O_2^{2-}	21
1127	clathrated O_2^-	21
3573	extraframework OH^-	22

characteristic of O_2^- ion.[21,23] An appreciable presence of the O^- radicals can be disregarded, since no clear feature at the diagnostic g = 2.05 value7,[24] was observed. More detailed analysis of the EPR spectra due to the O_2^- species via computer simulation (Fig. 4 dotted line) allowed for reliable extraction of the ***g***-tensor components (g_{zz} = 2.078, g_{yy} = 2.012, and g_{xx} = 2.005), which are in a nice accordance with earlier literature data.[18] The ***g***-tensor of the clathrated superoxide species is typical for surface modified $^2\Pi_{3/2}$ state,[21] characterized by the unpaired electron on the $|\pi^*(2p_x)\rangle$ antibonding orbital. The local C_{2v} crystal field gives rise to an orthorhombic ***g***-tensor with $g_{zz} >> g_{yy} > g_{xx} \approx g_e$ given by classic expressions:[25]

$$g_{xx} = g_e\left(\frac{\Delta^2}{\lambda_O^2+\Delta^2}\right)^{1/2} - \frac{\lambda_O}{E}\left[-\left(\frac{\lambda_O^2}{\lambda_O^2+\Delta^2}\right)^{1/2} - \frac{\Delta}{(\lambda_O^2+\Delta^2)^{1/2}} + 1\right] \quad (1)$$

$$g_{yy} = g_e\left(\frac{\Delta^2}{\lambda_O^2+\Delta^2}\right)^{1/2} - \frac{\lambda_O}{E}\left[\left(\frac{\lambda_O^2}{\lambda_O^2+\Delta^2}\right)^{1/2} - \frac{\Delta}{(\lambda_O^2+\Delta^2)^{1/2}} - 1\right] \quad (2)$$

$$g_{zz} = g_e + 2\left(\frac{\lambda_O^2}{\lambda_O^2+\Delta^2}\right)^{1/2} \quad (3)$$

where g_e = 2.0023, λ_O is the spin-orbit coupling constant, Δ is the splitting of both $\pi_g^*(2p_x)$ and $\pi_g^*(2p_y)$ levels, while E is the separation between the $\pi_g^*(2p_x)$ and $\sigma_g(2p_z)$ orbitals. The molecular λ and Δ parameters were derived from the experimental ***g***-tensor and collected in Table 2. The values of Δ = 0.44 eV and E = 3.04 eV are typical for superoxide radicals adsorbed on a divalent cation,[26] indicating that

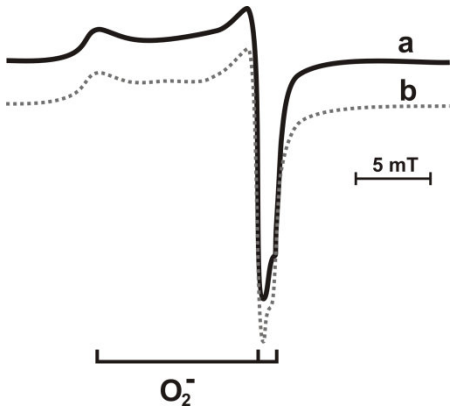

Fig. 4 X-band CW-EPR spectrum of pristine mayenite sample recorded at 77 K (solid line a - experimental, dotted line b - simulation).

Table 2 EPR parameters of copper(II) and superoxide species in mayenite obtained by computer simulation of the spectra

Paramagnetic center	***g***-tensor	Hyperfine tensor $^{Cu}\boldsymbol{A}$/MHz and molecular parameters
Cu^{2+} species A	$g_{xx} = 2.06 \pm 0.01$ $g_{yy} = 2.06 \pm 0.01$ $g_{zz} = 2.346 \pm 0.002$	$\lvert^{Cu}A_{xx}\rvert/h = 17 \pm 3$ $\lvert^{Cu}A_{yy}\rvert/h = 17 \pm 3$ $\lvert^{Cu}A_{zz}\rvert/h = 427 \pm 2$ $\alpha^2 = 0.80$, $\kappa = 0.40$
Cu^{2+} species B	$g_{xx} = 2.07 \pm 0.01$ $g_{yy} = 2.07 \pm 0.01$ $g_{z\,z} = 2.447 \pm 0.002$	$\lvert^{Cu}A_{xx}\rvert/h = 16 \pm 3$ $\lvert^{Cu}A_{yy}\rvert/h = 16 \pm 3$ $\lvert^{Cu}A_{zz}\rvert/h = 291 \pm 2$ $\alpha^2 = 0.75$, $\kappa = 0.40$
Cu^{2+} species C	$g_{xx} = 2.07 \pm 0.01$ $g_{yy} = 2.06 \pm 0.01$ $g_{zz} = 2.416 \pm 0.002$	$\lvert^{Cu}A_{xx}\rvert/h = 18 \pm 3$ $\lvert^{Cu}A_{yy}\rvert/h = 18 \pm 3$ $\lvert^{Cu}A_{zz}\rvert/h = 298 \pm 2$ $\alpha^2 = 0.65$, $\kappa = 0.42$
O_2^-	$g_{xx} = 2.005 \pm 0.002$ $g_{yy} = 2.012 \pm 0.002$ $g_{zz} = 2.078 \pm 0.002$	$\Delta = 0.44$ eV $E = 2.96$ eV $\lambda_O = 0.0168$ eV

superoxide species are indeed trapped at the Ca sites, in agreement with previous literature.[21] The λ_O value of 0.0168 eV, very close to the pure atomic one ($\lambda_0 = 0.0167$ eV), is pointing out that the encaged O_2^- radicals are stabilized on the Ca^{2+} centers essentially via through space electrostatic interactions. More detailed insight into the geometry of the stabilized superoxide species was inferred from the analysis of the pulse EPR data (vide infra).

The CW-EPR spectrum of the copper containing mayenite sample consists of four superimposed signals revealed by computer simulation (Fig. 5). Three of them (as it can be deduced from the presence of 3 distinct sets of hyperfine lines in the low field part) with apparently axial symmetry exhibit a well resolved "parallel" (z) hyperfine structure characteristic of Cu^{2+} ions ($S = 1/2$, $I = 3/2$). The "perpendicular" (x, y features) hyperfine coupling remained actually unresolved, even for the samples of the lowest copper loading. Therefore the data in Table 2 provide the best fit values for perpendicular parameters, assessed by computer simulation. In such case, precise determination of particular "$g_\perp$" and "$A_\perp$" values of the given contributing component signals is profoundly hampered, because of their strong mutual overlapping and broadening. The "$g_\perp$" values were all situated within the 2.06–2.07 range, and remained unresolved even at Q-band, whereas those of "$A_\perp$" varied from 16 to 18 MHz.

Broading of the EPR lines can be associated with the fluctuations in the ligand field caused by the disorder in the coordination sphere of copper. Indeed, as shown by Shluger,[27] extra-framework anions induce a strong structural relaxation of the corresponding cages, gauged by the interatomic distance between the axial Cu(Ca) ions (Fig. 1). The cage wall deformation is the strongest when the cage contains doubly charged O^{2-} anions (4.42 Å), for monovalent species (OH^-, O_2^-) it increases to 4.86 Å reaching the distance of 5.54 Å for empty cages. Such variations give rise to microheterogeneity of the copper structural environment, which is reflected in the EPR spectra. Strong interaction of the O^{2-} with Ca^{2+}/Cu^{2+} and cage wall Al^{3+} ions results in distinct displacement of those anions from the cage centre. In the case of extraframework

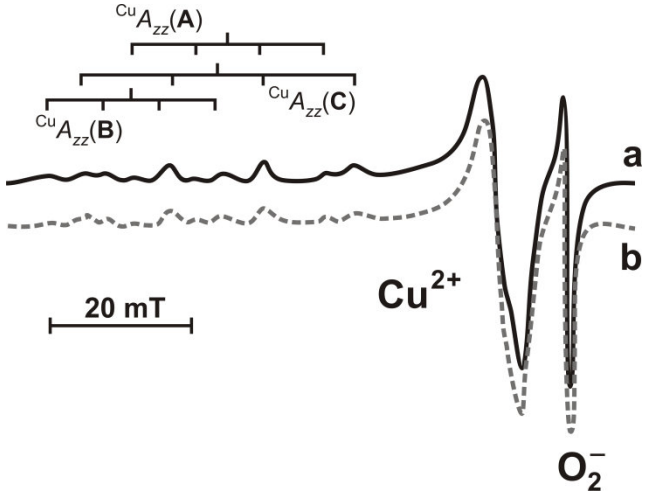

Fig. 5 X-band CW-EPR spectrum of Cu^{2+} and O_2^- species in copper containing mayenite (A, B, and C indicate three types of copper centers, solid line a – experimental spectrum, dotted line b – simulation).

OH^-, the oxygen atom is approximately at the cage centre, while the proton, oriented towards one of the cage wall oxygen ions, may form a hydrogen bond with it.[27] Thus, the resultant bonding anisotropy effect can be considered as a host site strain, smearing

out the perpendicular components to one broad feature.

The orthorhombic signal without hyperfine structure, emerging at the high field part (Fig. 5), belongs to the already described O_2^- radicals, with the g_{zz} component masked by the dominant perpendicular feature of the copper spectrum. All Cu signals were attributed to speciation of copper in the mayenite framework, reflecting the already mentioned irregularity of the two generic coordination polyhedra caused by the diversity of the extraframework anions. This attribution is supported by high sensitivity of the copper EPR spectrum to thermal treatment of the Cu-doped mayenite mixed with carbon soot in anaerobic conditions (Fig. S2, Supplementary Information). Such treatment leads to a gradual extraction of the extraframework oxygen, which is well reflected by the parallel part of the copper EPR spectra. Similar effect has previously been observed for Cu-exchanged zeolites, where simultaneous presence of several closely related copper species was also observed, and evolution of their relative abundance upon thermal treatment could be followed by EPR quite readily.[28]

As already mentioned two basic types of the $Cu_{Ca}^{\times}$ centers in the mayenite structure (shown in Fig. 1) exhibit local C_{2v} symmetry of the immediate environment, which by assuming that $\alpha|3d_{x^2-y^2}\rangle$ dominates in the SOMO, implies the following orthorhombic $\boldsymbol{A}$ tensor:[29]

$$A_{xx} = P\left[-\kappa\alpha^2 + \frac{2}{7}\alpha^2 + \Delta g_{xx} - \frac{3}{14}\Delta g_{yy}\right] \quad (4)$$

$$A_{yy} = P\left[-\kappa\alpha^2 + \frac{2}{7}\alpha^2 + \Delta g_{yy} - \frac{3}{14}\Delta g_{xx}\right] \quad (5)$$

$$A_{zz} = P\left[-\kappa\alpha^2 - \frac{4}{7}\alpha^2 + \Delta g_{zz} + \frac{3}{14}(\Delta g_{xx} + \Delta g_{yy})\right] \quad (6)$$

The σ-bonding coefficient α accounts for the covalency of the metal-ligand bond, $P = g_e\beta_e g_n\beta_n\langle r^{-3}\rangle = 0.036$ cm^{-1}, whereas κ reflects the Fermi contact term, and $\Delta g_{ii} = g_{ii} - g_e$. Unfortunately, as already discussed, due to broadening of the lines the splitting of the hyperfine tensor along x and y directions remains unresolved. Nonetheless, further data treatment becomes still workable upon assuming an apparent pseudoaxial symmetry ("$A_{\parallel}$" = A_z and "$A_{\perp}$" = $A_{xx} \approx A_{yy}$) for computer simulation of the EPR spectrum, since reliable distinction of both components is in such a case unfeasible. The best fit parameters and the corresponding calculated values of the α and κ coefficients are collected in Table 2. The obtained results are obviously approximate, yet still useful for primary account for the bonding situation of the $Cu_{Ca}^{\times}$ species.

The negative value of a_{iso} implies that spin polarization dominates over the direct contribution of $|4s\rangle$ orbital to the SOMO. The κ values are in the rather narrow range of 0.40 – 0.42, which is typically observed for copper ions in oxide hosts,[29] and confirms correct sign assignment of the hyperfine components. For estimation of the α^2 coefficients, we obtain 0.80, 0.75, and 0.65 for copper A, B, and C, respectively. The remaining part of the spin density is distributed over the oxygen ligands, indicating that the 3d orbitals of the $Cu_{Ca}^{\times}$ species are relatively contracted and contribute little to the bond covalency.

The observed $\boldsymbol{g}$-tensor is in full accordance with the results of the hyperfine structure analysis. Taking into account that $\alpha|3d_{x^2-y^2}\rangle$ dominates in the SOMO, so the minor quadratic terms can be ignored, we obtain the experimentally observed sequence $g_{zz} \approx g_e + 8\alpha^2\lambda_{Cu}/(E_{xy} - E_{x^2-y^2}) > g_{yy} \approx g_e + 2\alpha^2\lambda_{Cu}/(E_{xz} - E_{x^2-y^2})$, $g_{xx} \approx g_e + 2\alpha^2\lambda_{Cu}/(E_{yz} - E_{x^2-y^2})$, with $\lambda_{Cu} = 830$ cm^{-1}, and assuming an isotropic covalency coefficient α. [29] (The latter one can be derived from the analysis of the copper hyperfine structure). In accordance with these equations, speciation of copper is reflected in the case of the most sensitive g_{zz} value only.

Summarizing, the EPR data shows that the odd electron in Cu^{2+} is primarily localized on the $3d_{x^2-y^2}$ orbital overlapping with 2p orbitals of the in-plane oxygen ligands. The Cu–O bonds are rather ionic.

HYSCORE results

To investigate more deeply the coordination environment of

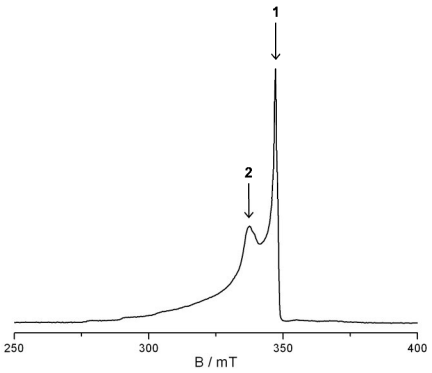

Fig. 6 Echo detected EPR spectrum of the investigated mayenite sample (π/2 = 16 ns, τ = 200 ns, T = 10 K). Arrows indicate the observer positions at which HYSCORE experiments were performed.

the Cu^{2+} and O_2^- ions, pulse EPR measurements were carried out. Fig. 6 shows the electron spin echo detected EPR spectrum for the same sample that was described in Fig. 5. As expected, the first derivative of the ESE-detected spectra (not shown) closely resembles the corresponding CW-EPR spectra. In order to unravel the details of the two paramagnetic species (Cu^{2+} and O_2^-) HYSCORE experiments were performed at two different magnetic field positions (see Fig. 6) corresponding to the Cu^{2+} and O_2^- perpendicular features. In both cases clear superhyperfine couplings are detected due to ^{27}Al and ^{1}H nuclei.

HYSCORE is a two-dimensional experiment where correlation of nuclear frequencies in one electron spin (m_S) manifold to nuclear frequencies in the other manifold is created by means of a mixing π pulse. ^{27}Al is a I = 5/2 nucleus with g_n = 1.4566, which means that the two electron spin manifolds α (m_s = 1/2) and β (m_s = –1/2) will split into six levels according to the nuclear spin quantum numbers, which range from m_I = 5/2 to m_I = –5/2. In general due to the nuclear quadrupole interaction these levels will be shifted proportionally to $(m_I)^2$. The HYSCORE spectrum for such a system will consist theoretically of $2(2I)^2$ = 50 correlation peaks for the $|\Delta m_I| = 1$ transitions and a number of cross peaks corresponding to $|\Delta m_I|$ = 2, 3, etc. However, the intensity of most of the correlation peaks is low and normally only single-double and double-double quantum transitions are observed in the experimental spectrum.[30]

The superoxide radical anion

The HYSCORE spectrum recorded at observer position 1 (Fig. 6) with B_0 = 347.0 mT, corresponding to the superoxide perpendicular feature is reported in Fig. 7. The spectrum is characterized by pronounced ridge patterns with major intensities at (3.58, 3.58) MHz, corresponding to the ^{27}Al

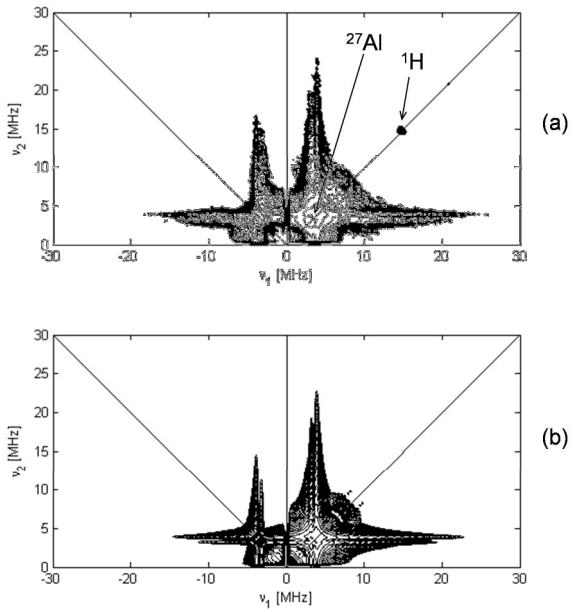

Fig. 7 a) HYSCORE spectrum taken at observer position B_0 = 347.0 mT (position 1 in Fig 6) with τ = 96, 168 ns and 0.25 kHz repetition rate; b) computer simulation considering two ^{27}Al nuclei with spin-Hamiltonian parameters reported in Table 3.

Table 3 Spin Hamiltonian parameters deduced from simulation of the HYSCORE spectra

Species	$^{H1}a_{iso}$ / MHz	^{H1}T / MHz	α, β, γ/°	$^{H2}a_{iso}$ / MHz	^{H2}T / MHz	α, β, γ/°	$^{Al}a_{iso}$ / MHz	^{Al}T / MHz	α, β, γ°	$\lvert e^2qQ/h\rvert$ / MHz	η
O_2^-	-	-	-	-	-	-	-0.5 ± 0.01	0.45 ± 0.01	0, 0, 0	9 ± 2	0.2 ± 0.1
	-	-	-	-	-	-	-0.2 ± 0.01	0.32 ± 0.01	0, 0, 0	3 ± 0.5	0.8 ± 0.1
Cu^{2+}	-2.63 ± 0.01	5.87 ± 0.05	0, 70 ± 20, 0	0.5 ± 0.2	0.9 ± 0.2	0, 30 ± 5, 0	-3.2 ± 0.5	1.1 ± 0.2	0, 30 ± 5, 0	9 ± 2	0.6 ± 0.1

Larmor frequency, compatible with a weak hyperfine coupling. The ridge patterns arise mainly from the quadrupolar interaction that leads to appearance of signals in the (–,+) quadrant. A signal centered at (ν_H, ν_H) is also observed in the (+,+) quadrant, which is due to the interaction of the superoxide radical anion with distant (matrix) ^{1}H. Because of the deep ^{27}Al modulation, suppression effects may prevent the detection of proton signals.[31] Therefore, ^{1}H matching HYSCORE experiments were carried out (see Fig. S3 in Supplementary Information), which failed to detect specific couplings to proximal protons of the OH^- ions. This fact can be rationalized considering that charge imbalance within the 3 adjacent mayenite cages has to be compensated by a single negative charge (e.g., due to extraframework OH^- or O_2^- ions) as described above in more detail. The presence of the O_2^- ion thus excludes the presence of OH^- groups within the same cage, leaving only remote OH^- protons trapped in the adjacent cages as source of the hyperfine coupling.

The CW-EPR spectrum of O_2^- ions adsorbed on Al^{3+} cations has been observed in the case of superoxide species stabilized on the surface of Al_2O_3 and is characterized by a $g_{zz} \cong 2.04$ and a maximum ^{27}Al hyperfine coupling of about 14.0 MHz.[32,33] These

values are clearly incompatible with both the observed g_{zz} = 2.0778 value (Fig. 4 and 5) and the experimental HYSCORE pattern reported in Fig. 7a, which is indicative of a ^{27}Al coupling of the order of 1 MHz. This nicely concurs with a study of Matsuishi et al.[34], who investigated the superoxide radicals in the mayenite single crystal. Based on isotopic enrichment and ESEEM experiments the authors proposed that the O_2^- is trapped in a side-on configuration on the Ca^{2+} ion. From the analysis of the mayenite structure it can be inferred that the superoxide species may interact weakly with up to eight Al ions. Under such circumstances the HYSCORE pattern reported in Fig. 7a can arise from different factors, namely the large nuclear spin of ^{27}Al (I = 5/2), the presence of multiple nuclei, and the quadrupolar interaction. We tried to rationalize these effects systematically with the help of computer simulations, based on the structural model reported elsewhere.[34] In particular, assuming O_2^- to be located in the middle point between two Ca^{2+} ions of the mayenite cavity, the superoxide anion will be surrounded by eight Al ions nearly equivalent at a distance of about 3.5 Å (Fig. 8). From this distance the dipolar coupling can be estimated within the framework of the point-dipole approximation yielding $2T$ = 0.96 MHz. The effects of a_{iso} and nuclear quadrupole interaction on the spectral pattern were then tested and are reported in the Supplementary Information (Fig. S4 and S5).

We assumed a_{iso} to be negative supposing a spin polarization mechanism, in agreement with theoretical calculations by Chuvylkin et al.[35] for nitroxides attached to Al^{3+} ions. We found that a maximum value for a_{iso} compatible with the experimental spectrum is of the order of 1.5 MHz. Any higher value is leading to the appearance of combination frequencies of the type (ν_α, $2\nu_\beta$) and (ν_β, $2\nu_\alpha$), which are not observed in the experimental spectrum.

The quadrupolar interaction plays a critical role in determining the spectral features, as shown in Fig. S5 of Supplementary Information. ^{27}Al quadrupole coupling data have been determined by means of MAS NMR spectra for polycrystalline $12CaO{\cdot}7Al_2O_3$ compounds.[36] Two different types of Al^{3+} ions are present in the mayenite cages, displaying different coordination structures, namely tetrahedral Al in AlO_4 distorted branching groups (Al(1) in Fig. 8) and undistorted AlO_4 tetrahedra with one non-bridging oxygen atom (Al(2) in Fig. 8). These differences lead to distinctly different quadrupole couplings, characterized by e^2qQ/h = 11 MHz and η = 0.2 for Al in distorted terahedra and e^2qQ/h = 3.2 MHz and η = 0.8 for the undistorted AlO_4. In our model the superoxide anion will interact with Al nuclei of both types (Fig. 8). In the simulation reported in Fig. 7b we thus considered the interaction with two types of ^{27}Al nuclei, characterized by the different quadrupole values and hyperfine parameters reported in Table 3. Due to the absence of distinct combination peaks in the experimental spectrum, it was not possible to ascertain the relative orientations of the nuclear quadrupole coupling tensors (see Fig. S6 in Supplementary Information). Despite this drawback the simulation is representative of the experimental spectrum, and points to a physical situation where the superoxide anion is stabilized within the mayenite cages by a Ca^{2+} ion and weakly interacting with two types of Al^{3+} ions forming the cage as shown in Fig. 8.

The Cu^{2+} cation

The HYSCORE spectrum recorded at observer position 2 (B_0 = 337.0 mT), corresponding to the Cu^{2+} perpendicular feature is reported in Fig. 9. The spectrum is characterized by a ridge pattern centered at (ν_H, ν_H), with maximum extension of about 9.1 MHz, indicating that, at variance with the O_2^- case, Cu^{2+} species strongly interact with nearby protons located in the

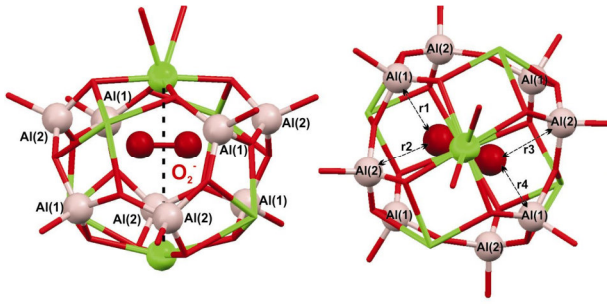

Fig. 8 Side and top views at the superoxide radical clathrated in a mayenite cage revealing two sets of four equivalent Al nuclei.

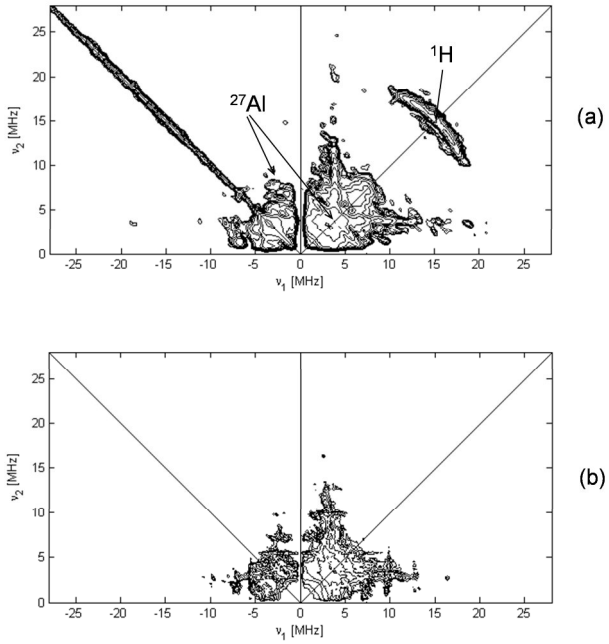

Fig. 9 a) HYSCORE spectrum taken at observer position B_0 = 337.0 mT, b) simulation obtained using the spin Hamiltonian parameters reported in Table 1. Three HYSCORE spectra were measured with τ = 96, 138, 172 ns added together. A 0.125 kHz repetition rate was used.

same cage. Moreover, the complex HYSCORE spectral pattern due to the ^{27}Al hyperfine interaction reveals important differences with respect to the spectra observed in correspondence to the O_2^- perpendicular features.

In particular a clear ridge with maximum extension of about 4.5 MHz is present in the (+,+) quadrant, together with well resolved cross peaks in the (–,+) quadrant at about (– 6.8, + 1.2) MHz and (– 1.2, + 6.8) MHz, which are indicative of an hyperfine coupling approaching the cancellation regime (i.e. $|A| \cong 2\nu_I$). This situation is similar to that observed by Carl et al.[30] in the case of Cu^{2+} ions in zeolite Y. Similarly to that case we find that the gross features of the experimental spectrum are accounted for by a relatively high a_{iso} value of the order of 3 MHz. A detailed analysis of the ^{27}Al HYSCORE spectrum shown in Fig. 9 is, however, a tantalizing exercise, as several contributions need to be taken into account. First of all three different Cu^{2+} species, with slightly different spin-Hamiltonian parameters contribute to the spectrum. Moreover, at the observer position at which the ^{27}Al HYSCORE spectrum was recorded, (corresponding to the Cu^{2+} $g_\perp$ feature) contributions from the O_2^- ions are also present at this field position.

The ^{27}Al ridge in the (+,+) quadrant displays a negligible shift with respect to the nuclear Larmor frequency, and no clear evidence of peaks associated with $\Delta m_I > 1$ was observed in the spectrum. This can be taken as an indication of a relatively small dipolar coupling.[37] The effect of an increasing dipolar coupling on the HYSCORE spectrum was tested by means of computer simulations (Fig. S7 of the Supplementary Information), which indicates that the intensity of multiquantum peaks becomes relevant for $T_\perp > 1.5$ MHz. These peaks are not observed in the experimental spectrum, and therefore we assume this as an upper value for the dipolar interaction. Based on this dipolar coupling we tested the effect of increasing a_{iso} on the spectral pattern and found that values of the order of 3 MHz are necessary to account for the cross peaks in the (–,+) quadrant. The nuclear quadrupole interaction then needs to be taken into consideration. In the previous section we found that two relatively large quadrupolar couplings are characteristic of ^{27}Al nuclei in the mayenite structure. The simulation with a relevant quadrupolar contribution (11 MHz) typical for these systems is reported in Fig. 9b, which qualitatively accounts for the observed experimental features (Table 3). Even though a univocal set of data could not be found, in all cases the peaks in the (–,+) quadrant could only be fitted with an a_{iso} value of the order of 3 MHz, which seems thus to be the distinctive feature of the spectrum. We remark that the parameters extracted from the simulation (Table 3) are in line with those found by Carl et al.[30,38] in the case of Cu^{2+} ions interacting with Al^{3+} ions in the framework of zeolite Y.

The presence of an isotropic hyperfine coupling indicates a direct bonding of the Cu^{2+} ions to the framework with significant spin density at the Al nucleus. The origin of the isotropic hyperfine coupling in this case stems from noticeable through bond interaction via polarization mechanism. Taking into account that the unpaired electron resides in the copper $3d_{x^2-y^2}$ orbital (vide supra), the overlapping with the oxygen framework orbitals leads to a spin density transfer to the Al nuclei. As a result of this bonding mechanism a negative spin density is expected at the Al nucleus. This has been indeed predicted by quantum chemical calculations relative to Cu^{2+} ions in zeolite framework and is consistent with the analysis of W band ENDOR spectra on similar systems.[38] The ^{27}Al hyperfine interaction thus directly shows the Cu^{2+}–framework interaction.

Another important information that stems from the HYSCORE spectrum is associated with the proton coupling. The ^{1}H ridge is

shown in Fig. 10a, (H1). An estimate of the maximum hyperfine coupling of A_{max} = 9.1 MHz can be deduced from the maximum extention of the ridge, measured parallel to one of the axes. Moreover, the proton ridge is clearly shifted from the (ν_H, ν_H) value, indicating a substantial dipolar interaction. Examination of the spectrum reveals that another proton ridge (H2 in Fig. 10a), with lower intensity and a maximum extension of about 3 MHz is also present. The different intensity ratio between the two proton ridges seems to indicate that they belong to different Cu^{2+} species with different aboundances, in accordance with the Cu^{2+} heterogeneity indicated by the simulation of the CW spectrum. We remark, however, that the different intensity of the two proton ridges may also be caused by the different modulation depth, which in turn depends on the anisotropy of the hyperfine couplings and on the number of approximately equivalent protons.

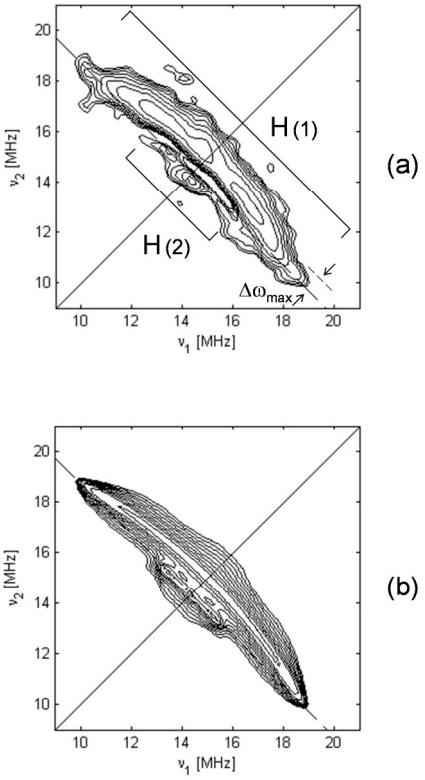

Fig. 10 Experimental (a) and simulated (b) HYSCORE spectra of the proton ridge. Experimental details are the same as reported in Fig. 9.

The shape of the dominant ridge pattern (H1) requires that $a_{iso} < T_\perp$ and is characteristic of protons located within the $g_\perp$ plane of Cu^{2+} ions.[39] Under these circumstances it has been shown[39,40] that for ^{1}H HYSCORE spectra taken at the $g_\perp$ position, the maximum shift of the proton ridge, $\Delta\omega^s_{max}$, from the diagonal is directly correlated to the magnitude of the $T_\perp$ coupling, according to equation (7).

$$\Delta\omega_{max} = \frac{9T^2}{32|\omega_I|} \tag{7}$$

Considering that $\Delta\omega^s_{max}$ =0.69 MHz and that the maximum extension of the ridge corresponding to $|a_{iso} + 2T|$ = 9.1 MHz, the values of a_{iso} and T can be estimated, even though a single observer position was sampled, corresponding to the $g_\perp$ position of the EPR spectrum. Assuming the sign of T as positive (g_n = 5.58569 for H), $T \cong 5.5$ MHz was obtained. This value was used as a starting point for the simulation of the proton ridge shown in Fig. 10b, and refined to a_{iso} = – 2.63 MHz and T = 5.87 MHz (Table 3). The Euler angle β is found to be in the range of 50° – 90°. A more accurate determination of its value was hampered by the low signal to noise ratio at the observer position corresponding to $g_\parallel$. The extracted values are, however, clearly indicative of an equatorially bound OH^- group.[39,41] The negative sign for the Fermi contact term can be qualitatively understood on the basis of a spin polarization mechanism, considering that the unpaired electron dwells in a molecular orbital which is mainly $3d_{x^2-y^2}$ in character (with small admixtures of oxygen non-bonding orbitals). A similar situation holds in the case of the $Cu(H_2O)_6^{2+}$ complex.[42]

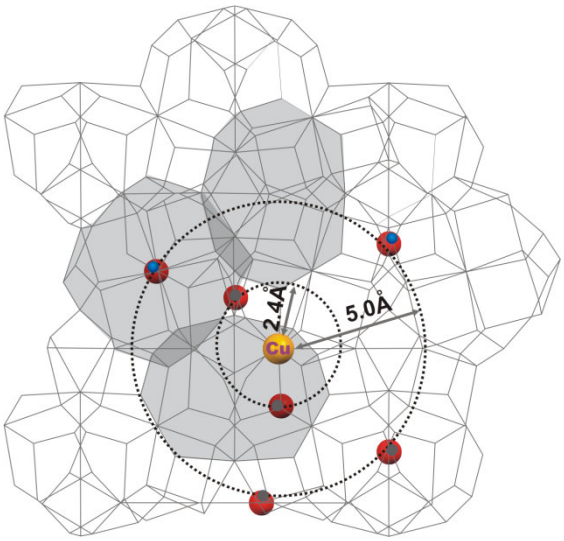

Fig. 11 Fragment of the mayenite structure showing possible location of proximal (at distance of 2.4 Å) and distal (at distance of 5.0 Å) protons, located in the same and the nearby cages, respectively.

The second proton ridge is far less well resolved, however, computer simulation (Fig. 10b) indicates that $|a_{iso}|$ = 0.5 MHz and $|T|$ = 0.9 MHz led to the results compatible with the experimental spectrum.

Assuming that the anisotropic part of the hyperfine interaction can be described as a purely point-dipolar interaction, the distance between the two differently coupled protons and the Cu^{2+} cation can be estimated from equation (8):

$$T = \frac{\mu_0}{4\pi} g_e g_n \beta_e \beta_n \frac{1}{r^3} \qquad (8)$$

The resulting values were found to be 2.4 ± 0.1 Å and 5.0 ± 0.5 Å for the strongly and weakly coupled protons, respectively. We should remark that in the case of the weakly coupled proton, due to the poor quality of the signal, the assignment should be taken as tentative.

From the structural data extracted from the HYSCORE spectra and the geometrical constraints imposed by the mayenite structure (Fig. 11) the strongly coupled protons can be assigned to an OH^- group equatorially bound to the Cu^{2+} ions. The presence of an OH^- group is required in order to maintain the charge balance of the system.

Conclusions

A combination of CW-EPR and HYSCORE spectroscopies was used to characterize the local environment of Cu^{2+} and O_2^- species localized within the cages of nanoporous $12CaO{\cdot}7Al_2O_3$. Three different Cu^{2+} species were identified by means of CW-EPR, and were associated with structural modifications of the copper host polyhedron caused by alterable extra-framework anions (O_2^-, O_2^{2-}, OH^-). HYSCORE spectra revealed clear superhyperfine interactions of the Cu^{2+} ions with proximal (2.4 Å) and distal (5.0 Å) OH^- anions, located in the same and the nearby cage, respectively. In the case of the O_2^- ions evidence was provided for the encapsulation in the proton free cavities and preferential interaction with the Ca^{2+} ions.

Acknowledgements

This work was supported by COST action D41 and 299/N-COST/208/0 project of MNiSzW. M.R. acknowledges Project operated within the Foundation for Polish Science – Ventures Programme – co-financed by the EU European Regional Development Fund, project no. Ventures/2008-2/4 ("*The catalyst for high-temperature nitrous oxide decomposition in nitric acid installations*"). M.C. acknowledges funding from Regione Piemonte through the DAMMONEU06 project. The research was partially carried out with the equipment purchased thanks to the financial support of the European Regional Development Fund in the framework of the Polish Innovation Economy Operational Program (Contract No. POIG.02.01.00-12-023/08).

Notes and references

[a] *Dipartimento di Chimica IFM, Università di Torino, and NIS Centre of Excellence, via P. Giuria 7, 10125 Torino, Italy. E-mail: m.chiesa@unito.it*
[b] *Faculty of Chemistry, Jagiellonian University, ul. Ingardena 3, 30-060 Krakow, Poland. E-mail: sojka@chemia.uj.edu.pl*

† Electronic Supplementary Information (ESI) available: Effect of increasing a_{iso}, dipolar, and quadrupolar tensors on the ^{27}Al HYSCORE spectrum, as well as ^{1}H matched HYSCORE spectrum.

1 Y. Jun, J. Choi and J. Cheon, *Angew. Chem. Int. Ed*., 2006, **45**, 3414.
2 X. Chen and S. S. Mao, *Chem. Rev*., 2007, **107**, 2891.
3 F. Schuth*, Annu. Rev. Mater. Res*., 2005, **35**, 209.
4 A. Henglein, *Chem. Rev*,. 1989, **89**, 1061.
5 J. V. Stark, and K. J. Klabunde*, Chem. Mater*., 1996, **8**, 1913.
6 M. Lacerda, J. T. S. Irvine, F. P. Glasser and A. R. West, *Nature,* 1988, **332**, 525.
7 H. Hosono, *Sci. Technol. Adv. Mater*., 2004, **5**, 409.
8 K. Hayashi, N. Ueda, M. Hirano and H. Hosono, *Solid State Ionics,* 2004, **173**, 89.
9 H. Hosono and Y. Abe, *Inorg. Chem*., 1987, **26**, 1192.
10 S. Matsuishi, K. Hayashi, M. Hirano, I. Tanaka and H. Hosono, *J. Phys. Chem. B*, 2004, **108**, 1857.
11 M. Ruszak, M. Inger, S. Witkowski, M. Wilk, A. Kotarba and Z. Sojka, *Catal. Lett*., 2008, **126**, 72.
12 S. Fujita, H. Nakano, K. Suzuki, T. Mori and H. Maruda, *Catal. Lett*., 2006, **106**, 139.
13 K. Sato, M. Yamaguchi, S. Fujita, K. Suzuki and T. Mori, *Catal. Commun*., 2006, **7**, 132.
14 T. Spałek, P. Pietrzyk and. Z. Sojka*, J. Chem. Inf. Model*., 2005, **45**, 18.
15 P. Höfer, A. Grupp, H. Nebenfür and M. Mehring, *Chem. Phys. Lett*., 1986, **132**, 279.
16 Z. L. Madi, S. Van Doorslaer and A. Schweiger, *J. Mag. Reson.* 2002, **154**, 187.
17 H. Boysen, M. Lerch, A. Stys and A. Senyshyn, *Acta Cryst*. 2007, **B63**, 675.
18 M. Ruszak, S. Witkowski and Z. Sojka, *Res. Chem. Intermed*., 2007, **33**, 689.
19 S. Yang, N. Kondo, K. Hayashi, M. Hirano, K. Domen and H. Hosono, *Chem. Mater*., 2004, **16**, 104.
20 K. Kajihara, S. Matsuishi, K. Hayashi, M. Hirano and H. Hosono, *J. Phys. Chem. C*, 2007, **111**, 14855.
21 M. Che and A. J.Tench, *Adv. Catal*., 1983, **32**, 1.
22 K. Hayashi, P. V. Sushko, D. M. Ramo, A. L. Shluger, S. Watauchi, I. Tanaka, S. Matsuishi, N. Ueda, M. Hirano and H. Hosono, *J. Phys. Chem. B*, 2007, **111**, 1946.
23 Z. Sojka, *Catal. Rev. Sci. Eng*., 1995, **37**, 461.
24 K. Hayashi, S. Matsuishi, N. Ueda, M. Hirano and H. Hosono, *Chem. Mater*., 2003, **15**, 1851.
25 W. Kanzig, M. H. Cohen, *Phys. Rev .Lett*., 1959 **3**, 509.
26 M. Chiesa, M. C. Paganini, E. Giamello and D. M. Murphy, *Langmuir,* 1997, **13,** 5306.
27 P. V. Sushko, D. Munoz Ramo, A. L. Shluger, *Phys. Stat. Sol*. (a), 2007, **204**, 663.
28 R. A Schoonheydt, *Catal. Rev. Sci. Eng.*, 1993, **35**, 129.
29 F. E. Mabbs and D. Collison, *Electron Paramagnetic Resonance of d Transition Metal Compounds*, Elsevier, Amsterdam, 1992.
30 P. J. Carl, D. E. W. Vaughan and D. Goldfarb, *J. Phys. Chem. B,* 2002, **106**, 5428.
31 S. Stoll, C. Calle, G. Mitrikas, A. Schweiger *J. Mag. Reson. 2005*, **177**, 93.
32 M. Che, J. C. McAteer and A. J. Tench, *Chem. Phys. Lett.,* 1975, **31**, 145.
33 D. B. Losee, *J. Catal.,* 1977, **50**, 545.
34 S. Matsuishi, K. Hayashi, H. Masahiro, I. Tanaka and H. Hosono, *J. Phys. Chem. B,* 2004, **108**, 18557.
35 N. D. Chuvylkin, A. M. Tokmachev, A.V. Fionov and E. V. Lunina, *Russ. Chem. Bullettin*, 1997, **46**, 1649.
36 D. Muller, W. Gessner, A. Samoson, E. Lippmaa and G. Scheler, *Polyhedron*, 1986, **5**, 779.
37 M. Gutjahr, R. Bottcher, A. Pöppl, *Appl. Magn. Reson.* 2002, **22**, 401.
38 P. J. Carl, D. E. W. Vaughan, D. Goldfarb, *J. Am. Chem. Soc,* 2006, **128**, 7160.
39 A. Pöppl, L. Kevan, *J. Phys. Chem*., 1996, **100**, 3387.
40 A. Schweiger, G. Jeschke, *Principles of Pulse Electron Paramagnetic Resonance*, 2001, Oxford University Press, Oxford, U.K.
41 A. Pöppl, M. Newhouse, L. Kevan, *J. Phys. Chem*., 1995, **99**, 10019.
42 N. M. Atherton, A. J. Horsewill, *Mol. Phys.* 1979, **37**, 1349.